Journal of Power Sources 196 (2011) 7728–7735

Contents lists available at ScienceDirect

Journal of Power Sources

journal homepage: www.elsevier.com/locate/jpowsour

Optimized performances of core–shell structured $LiFePO_4$/C nanocomposite

W.L. Liu, J.P. Tu*, Y.Q. Qiao, J.P. Zhou, S.J. Shi, X.L. Wang, C.D. Gu

State Key Laboratory of Silicon Materials and Department of Materials Science and Engineering, Zhejiang University, Hangzhou 310027, China

ARTICLE INFO

Article history:
Received 31 March 2011
Received in revised form 30 April 2011
Accepted 17 May 2011
Available online 27 May 2011

Keywords:
Lithium iron phosphate
Poly(vinyl alcohol)
Carbon-shell
Diffusion coefficient
Low temperature

ABSTRACT

A nanosized $LiFePO_4$/C composite with a complete and thin carbon-shell is synthesized via a ball-milling route followed by solid-state reaction using poly(vinyl alcohol) as carbon source. The $LiFePO_4$/C nanocomposite delivers discharge capacities of 159, 141, 124 and 112 mAh g^{-1} at 1 C, 5 C, 15 C and 20 C, respectively. Even at a charge–discharge rate of 30 C, there is still a high discharge capacity of 107 mAh g^{-1} and almost no capacity fading after 1000 cycles. Based on the analysis of cyclic voltammograms, the apparent diffusion coefficients of Li ions in the composite are in the region of 2.42×10^{-11} cm^2 s^{-1} and 2.80×10^{-11} cm^2 s^{-1}. Electrochemical impedance spectroscopy and galvanostatic intermittent titration technique are also used to calculate the diffusion coefficients of Li ions in the $LiFePO_4$/C electrode, they are in the range of 10^{-11}–10^{-14} cm^2 s^{-1}. In addition, at −20 °C, it can still deliver a discharge capacity of 122 mAh g^{-1}, 90 mAh g^{-1} and 80 mAh g^{-1} at the charge–discharge rates of 0.1 C, 0.5 C and 1 C, respectively.

1. Introduction

With the shortage of fossil fuels and severe global warming, electric vehicles (EVs) and hybrid electric vehicles (HEVs) attract more and more attention [1,2]. Among these devices, lithium-based batteries are the most promising candidates in terms of energy density, although the achievement of high power density is hindered by kinetic problems of the electrode materials [1–6]. The layered $LiCoO_2$ as cathode material has been commercialized, but it shows relatively low safety [7,8]. So it was soon replaced by the potential candidate olivine lithium iron phosphate ($LiFePO_4$) because of its high theoretical capacity (170 mAh g^{-1}), long life, acceptable operating voltage (3.4 V vs. Li^+/Li), high safety, environmental compatibility and low cost [8–22].

However, $LiFePO_4$ has low electronic and ion conductivities [8,21], low tap density, and poor low-temperature character [23]. A large number of efforts have been made to overcome the electronic and ionic transport limitations by doping with supervalent cations, incorporating nanostructured designs, or coating electronically conductive agents [9–19]. Recently, mesoporous structure and microsphere have been increasingly applied to improve the electrochemical performance of $LiFePO_4$ [24–30]. It is difficult to make sure whether the supervalent ion occupy the Li or Fe site, and the supervalent cation doping is not necessarily improving the performance of $LiFePO_4$ [31]. Only good carbon-coating and nanosized $LiFePO_4$ could efficiently improve the performance of $LiFePO_4$ and allow for high absolute capacities [32,33]. But the surface of $LiFePO_4$ could not be coated completely in some researches and the thickness of carbon layer was not homogeneous [34]. Meanwhile, it was not always the higher amount of carbon coated on $LiFePO_4$ particles, the better performance of the electrode [13]. The thick carbon layers would affect the contact of electrolyte and electroactive materials and then block the Li-ion transporting across the electrolyte/electrode interface [35,36]. In addition, high carbon content would decrease the energy density unduly which was considered with equal importance as rate capability in practical applications [37].

The traditional but simple solid-state reaction method is often used to synthesize the $LiFePO_4$/C composite. Herein the complete, homogeneous, thin coating of carbon ensures that the $LiFePO_4$ particles can get electrons from all directions and the Li-ions can penetrate through the carbon coating without appreciable polarization [33]. Although poly(vinyl alcohol) (PVA) had been used as carbon source to synthesize $LiFePO_4$/C by several research groups [38–42], either their sintering temperatures or the carbon amounts were high. In this work, the $LiFePO_4$/C composites are synthesized via a ball-milling route followed by solid-state reaction. To optimize the electrochemical performances, a nanosized $LiFePO_4$/C composite containing the carbon-shell with a thickness of 1.3 nm is obtained through pre-sintering process. The electrochemical properties of the $LiFePO_4$/C composite are investigated, presenting excellent rate capability and cycling stability. In addition, the diffusion coefficients of lithium ions in $LiFePO_4$/C are also simultaneously determined by cyclic voltammetry (CV), electrochemical impedance spectroscopy (EIS) and galvanostatic intermittent titration technique (GITT) methods.

* Corresponding author. Tel.: +86 571 87952856; fax: +86 571 87952573.
E-mail address: tujp@zju.edu.cn (J.P. Tu).

0378-7753/$ – see front matter © 2011 Elsevier B.V. All rights reserved.
doi:10.1016/j.jpowsour.2011.05.046

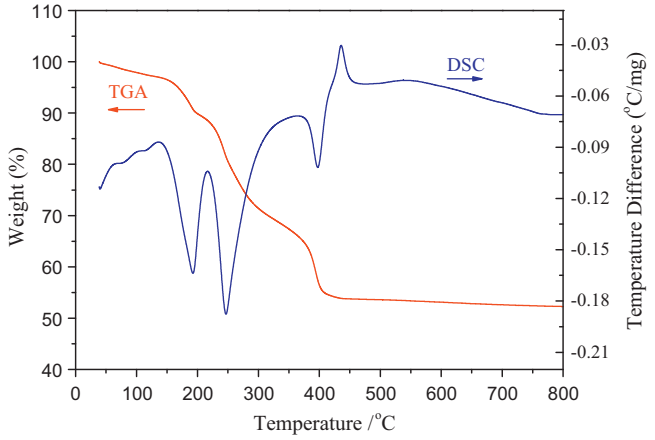

Fig. 1. DSC–TGA curves of $LiFePO_4$/C precursor recorded from room temperature to 800 °C at a heating rate of 10 °C min^{-1} under an Ar flow of 120 ml min^{-1}.

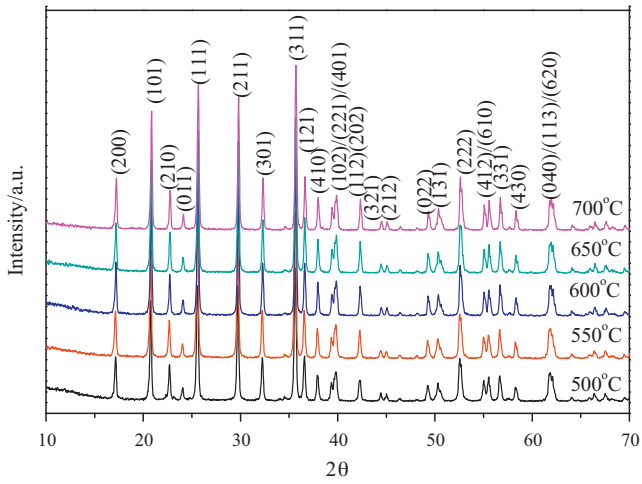

Fig. 2. XRD patterns of $LiFePO_4$/C synthesized at different temperatures.

2. Experimental

The carbon-shell coated $LiFePO_4$ was synthesized using a ball-milling route followed by solid-state reaction. In a typical synthesis, stoichiometric Li_2CO_3, $FeC_2O_4{\cdot}2H_2O$ and $NH_4H_2PO_4$ and 2.5 wt.% of PVA as the carbon source was mixed by ball-milling at a high speed of 500 rpm, which first dry-milling, then wet-milling using ethanol as solvent. Ball-milling was carried out at room temperature in air using zirconia vials and balls. After evaporating the ethanol, the PVA-containing precursor was ground using mortar and pestle, and pelleted, then heated in a pure nitrogen atmosphere at 350 °C. Afterwards, the decomposed precursor was reground, pressed into pellets and sintered at the temperatures ranging from

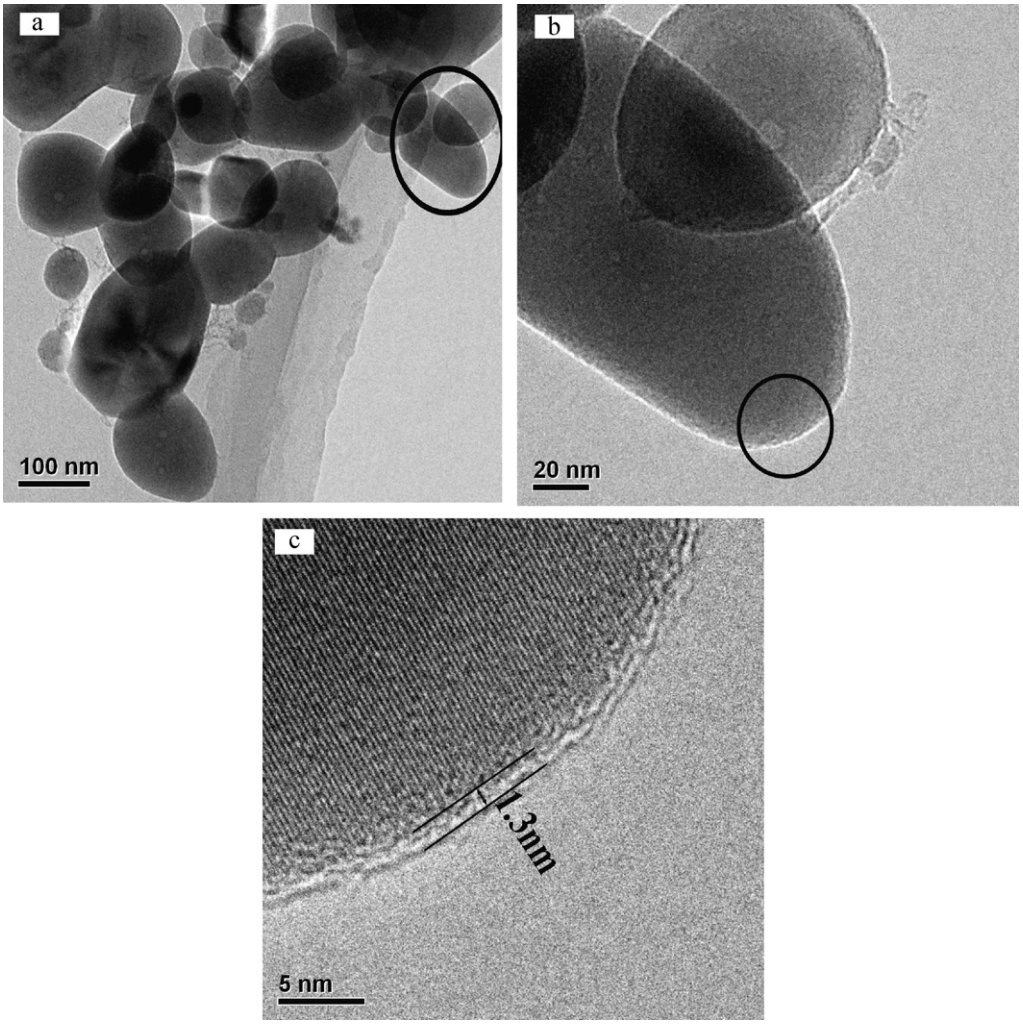

Fig. 3. (a and b) TEM and (c) HRTEM images of $LiFePO_4$/C synthesized at 600 °C.

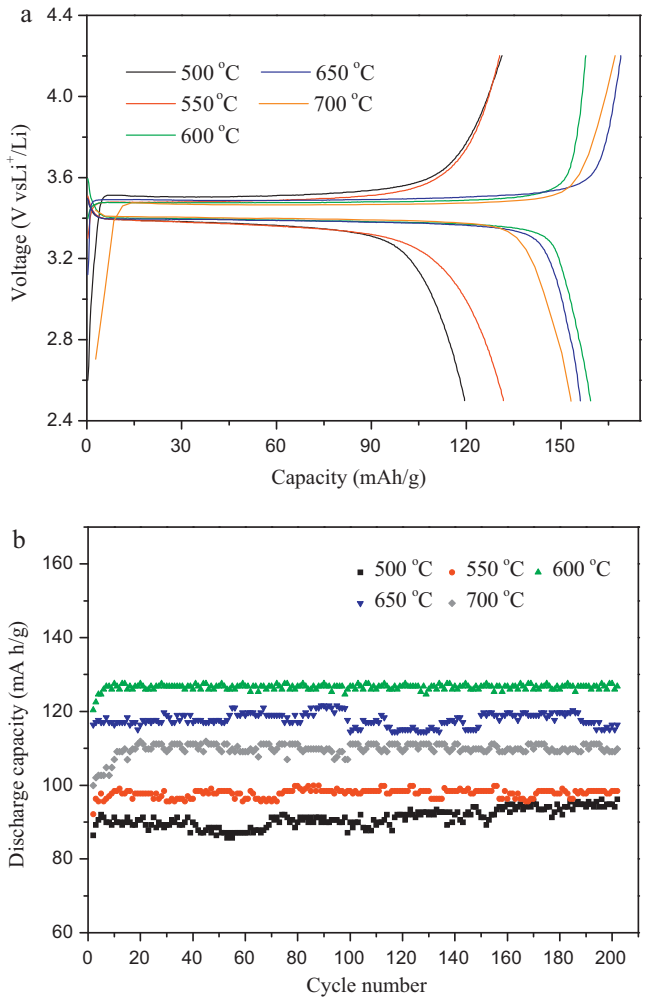

Fig. 4. (a) The first charge–discharge curves at 1 C and (b) cycling performance at 15 C of $LiFePO_4$/C synthesized at different temperatures between 2.5 and 4.2 V.

500 °C to 700 °C for 8 h in a nitrogen–argon mixture to get $LiFePO_4$/C composite.

The thermal behavior of the PVA-containing mixture was examined by DSC–TGA analysis using SDT Q600 V8.2 Build 100 instrument from 0 °C to 800 °C at a heating rate of 10 °C min^{-1} in a nitrogen atmosphere. The structure of the $LiFePO_4$/C composites was characterized by X-ray diffraction (XRD, Philips PC-APD with Cu Kα radiation). The morphology of carbon-shell coated on $LiFePO_4$ was identified by a transmission electron microscopy (TEM, JEOL JEM-2010F). The actual carbon content in the $LiFePO_4$/C material was measured by means of an automatic elemental analyzer (EA, Flash EA1112).

Electrochemical performances were performed by assembling CR2025 coin cells for galvanostatic charge–discharge testing. The cell consisted of a lithium foil anode and a $LiFePO_4$/C cathode separated by a polypropylene microporous separator (Cellgard 2300), 1 M $LiPF_6$ in ethylene carbonate (EC)–diethyl carbonate (DEC) (1:1 in volume) as the electrolyte (the electrolyte was LB-302, which was purchased from Zhangjiagang Guotai-Huarong New Chemical Materials Co.). The cathode was made of 80 wt.% $LiFePO_4$/C, 4 wt.% polyvinylidene fluoride (PVDF) as a binder and 16 wt.% acetylene black, which were dispersed in 1-methyl-2-pyrrolidinone(NMP), and the resultant slurry was then spread onto an a circular disc aluminum foil. After drying in an oven at 60 °C, the cathode was pressed to achieve good adherence between the coated material and the aluminum foil. The coin cells were assembled inside a glove box filled with high-purity argon gas (99.9995% purity). The galvanostatic charge–discharge tests were conducted on LAND battery program-control test system at different rates at room temperature and at −20 °C in the voltage range of 2.5–4.2 V. GITT tests were also conducted on this apparatus at room temperature in the voltage range of 2.8–4.0 V. The Bitrode unit was programmed to supply a constant current flux (C/20) for 10 min to the cell followed by open circuit stand for 40 min. CV were performed on CHI660C electrochemical workstation in the potential ranges of 2.0–4.5 V (vs. Li/Li^+) at room temperature and at −20 °C, respectively, at the scan rates from 0.1 to 2.0 m s^{-1}. For EIS measurements, the test cells were three-electrode cells with the metallic lithium foil as both the reference and counter electrodes. The EIS measurements were performed on CHI660C electrochemical workstation over a frequency range of 100 kHz–10 mHz at different charge–discharge stages by applying an AC signal of 5 mV.

3. Results and discussion

Fig. 1 shows the DSC–TGA curves of the precursor containing PVA in a nitrogen gas flow. There is about 3 wt.% weight loss below 160 °C which corresponds to the removal of adsorbed water. There is a continuous weight loss when heated to 450 °C due to decomposition of $FeC_2O_4{\cdot}2H_2O$, $NH_4H_2PO_4$, Li_2CO_3 and PVA, which correspond with the endothermic peaks in the DTA curve at 192.5 °C, 247.1 °C, 397.5 °C, respectively. Therefore, during the pre-sintering process at 350 °C for 5 h, the raw materials decomposed and emitted gases from decomposition reaction, meanwhile it companied with PVA melting and caused the PVA to foam or intumesce which could penetrate into the decomposed materials and mixed with them more sufficiently [43]. Thereafter the mass remains almost constant up to 800 °C, indicating the formation of product from the temperature at 450 °C, as is also evidenced by the exothermic peak at 435.7 °C in the DTA curve. Above 500 °C, there is hardly any weight loss, so we choose 500 °C as the initial sintering temperature.

Fig. 2 shows the XRD patterns of $LiFePO_4$/C synthesized at different temperatures. After sintering between 500 and 700 °C, well-crystallized $LiFePO_4$ can be obtained. The diffraction peaks are in full accord with the ordered $LiFePO_4$ olivine structure indexed by orthorhombic Pnmb (JCPDS Card No. 83-2092). With the sintering temperature increasing from 500 °C to 700 °C, there is only a little difference in the XRD patterns, suggesting that complete crystal growth of $LiFePO_4$ can be achieved at relatively low temperature. No peak corresponding to the carbon is observed due to its low content and amorphous state. The actual carbon contents in the final products measured by means of an automatic elemental analyzer was found to decrease from 1.76 wt.% to 1.09 wt.% with the increase of sintering temperature from 500 °C to 700 °C.

In order to check the carbon distribution in the powder, TEM and HRTEM analysis of the $LiFePO_4$/C composite synthesized at 600 °C were conducted, as shown in Fig. 3. In Fig. 3a and b, it can be seen that the particles are sphere-like and well-dispersed with fine sizes of 50–150 nm. There is only a little of carbon network in the interstitial grain boundary region, which can meet the electrical continuity between the $LiFePO_4$ crystallites. The HRTEM image of the $LiFePO_4$/C nanocomposite is shown in Fig. 3c. It clearly reveals that the carbon-shell coated on the highly crystalline $LiFePO_4$ is very thin, and the thickness of carbon-shell is about 1.3 nm. This carbon-shell is helpful to the improvement of electron conductivity as well as the Li-ion diffusion, because of the short distance between the active material and the electrolyte. Such intact and uniform carbon shell may be attributed to the pre-sintering process at 350 °C for 5 h. At 350 °C, the H_2O in PVA was eliminate completely, and the raw materials almost decomposed completely too

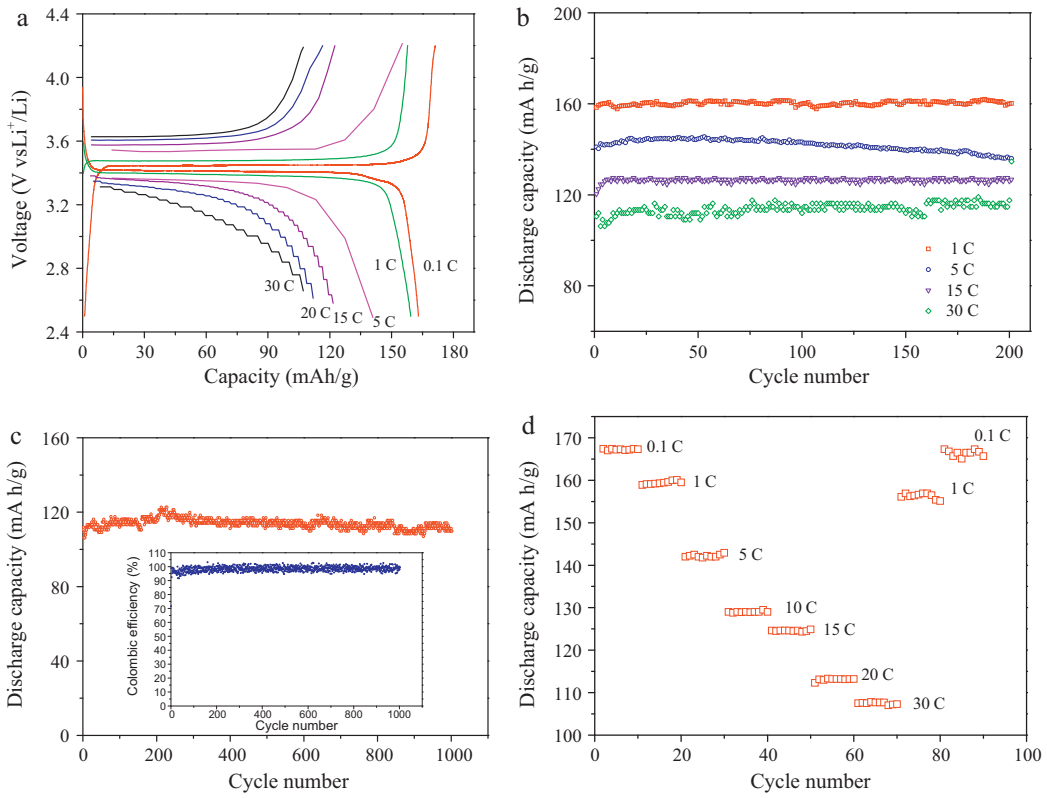

Fig. 5. (a) The first charge–discharge curves and (b) cycling performance of $LiFePO_4$/C synthesized at 600 °C tested at different rates between 2.5 and 4.2 V, (c) cycling profile tested at 30 C, the inset shows the high coulombic efficiency, and (d) rate performance of $LiFePO_4$/C at different current rates.

[43]. During the emission of the gases, the chain polyenes from the elimination reaction would wrap the decomposed precursor, and the subsequent calcination made polyenes carbonize and formed $LiFePO_4$ crystal at the same time. Therefore, the carbon can coat on the $LiFePO_4$ particles entirely and uniformly. Meanwhile, the foaming or intumescing caused by melting and decomposition would allow the decomposer to be freely and sufficiently mixed with the raw materials after sintering at 350 °C.

Fig. 4a shows the initial charge–discharge curves of $LiFePO_4$/C at a rate of 1 C. Their discharge capacities are 119, 131, 159, 155 and 153 mAh g^{-1}, corresponding to the sintering temperature 500 °C, 550 °C, 600 °C, 650 °C and 700 °C, respectively. Therefore, for the sample synthesized at 600 °C, the discharge flat plateau is the longest, and its initial coulombic efficiency is about 100%. The difference between the charge and the discharge voltage is only about 0.1 V, which is representative of its good kinetics, especially on consideration of the low electrochemical diffusion rate of lithium ions in a solid phase. Fig. 4b shows the cycle performance of the $LiFePO_4$/C composites synthesized at different temperatures at a charge–discharge rate of 15 C. They are all stable during the 200 cycles. The $LiFePO_4$/C composite synthesized at 600 °C exhibits the highest capacity of 124 mAh g^{-1} and the best cycle performance in which has no capacity fading after the 200th cycle. This best performance may be due to its higher crystallinity compared with the composites synthesized at 500 °C and 550 °C, and higher carbon amount and smaller sizes compared with the ones synthesized at 650 °C and 700 °C.

Fig. 5a shows the first charge/discharge curves of $LiFePO_4$/C synthesized at 600 °C at various rates. The electrode delivers a discharge capacity of 165 mAh g^{-1} at 0.1 C, which is very close to the theoretical capacity of $LiFePO_4$ (170 mAh g^{-1}). Even at the high current rates of 5 C, 15 C, 20 C, 30 C, the $LiFePO_4$/C electrode still obtains high discharge capacities of 141 mAh g^{-1}, 124 mAh g^{-1}, 112 mAh g^{-1}, 107 mAh g^{-1}, respectively, demonstrating that the as-synthesized nanocomposite can endure high-rate charge and discharge. The rate performance of our $LiFePO_4$/C far exceeds those of the previously reported $LiFePO_4$/C composites with PVA as carbon sources [38–42], as shown in Table 1. This is mainly due to the optimized pre-sintering temperature (350 °C) and carbon content (about 1.5 wt.%).

The $LiFePO_4$/C electrode can not only supply large capacity, but also maintain good cycle life at high charge–discharge rates. As shown in Fig. 5b, the discharge capacities maintain 160, 136, 126 and 111 mAh g^{-1} after 200 cycles at 1 C, 5 C, 15 C and 30 C rates, respectively. What's more, the cell also maintains high columbic efficiency, with an average value of about 99.5% over 1000 cycles at a charge–discharge rate of 30 C, revealing superior cycling stability (Fig. 5c). This can meet the requirement to operate at high current density and to have a cycle life more than 5000 cycles in the HEV or PHEV application [37]. Fig. 5d shows the influence of the change in charge–discharge rate on the capacity retention. The results show that the capacity has only a little fading when the discharge rate returns from 0.1 C to 30 C. This demonstrates that the $LiFePO_4$/C nanocomposite is able to tolerate various discharge currents, which is desirable for high power applications.

Fig. 6a shows the CV profiles of $LiFePO_4$/C electrode between 2.0 and 4.5 V at different scanning rates. A couple of redox peaks are observed between 3.36 and 3.53 V in the CV curve obtained at a scanning rate of 0.1 mV s^{-1}. These peaks correspond to the extraction and insertion of lithium ions. The height and area of the redox peaks increase with the increase of the scanning rates. Meanwhile, the cathodic and anodic peaks move to the lower and higher potentials, respectively. This indicates that the irreversible behaviors become more evident due to the electrode polarization at larger scan rates. But the very well-defined sharp redox reaction peaks are still maintained even at the high scanning rate of 2.0 mV s^{-1}.

Table 1
Comparison of $LiFePO_4$/C using PVA as carbon source.

Method	Sintering temperature (°C)	Carbon content (wt.%)	The best performance	Ref.
Solid-state reaction	800	5	153 mA g^{-1} at 0.1 C, 120 mA g^{-1} at 1 C	[38]
SD-post-annealing	600	5.1	139.4, 137.2, 133.5, 127.3 mA g^{-1} at 0.2, 1, 5, 10 C, respectively	[39]
Sonochemical	600	5	124 mA g^{-1} at 0.1 C, 115 mA g^{-1} at 3 C	[40]
Ceramic granulation	700	5	145 mA g^{-1} at 0.1 C, 80 mA g^{-1} at 3 C	[41]
CVD-solid state	700	10.9	155 mA g^{-1} at 0.1 C, 138 mA g^{-1} at 1 C	[42]
Solid-state reaction route	600	1.5	165, 159, 141, 107 mA g^{-1} at 0.1, 1, 5, 30 C, respectively	This work

The peak current I_p (Amperes), during anodic scans at different scanning rates are used to extract the Li-ion diffusion coefficient D ($cm^2\ s^{-1}$), applying the Randles Sevcik equation [44]:

$$I_p = 2.69 \times 10^5 A C D^{1/2} n^{3/2} v^{1/2} \quad (1)$$

where A is the interface between the electrolyte and the active material, C is the shuttle concentration (mol cm^{-3}), n is the number of electrons involved in the redox process ($n = 1$ for Fe^{2+}/Fe^{3+} redox pair), and v is the potential scan rate (V s^{-1}). As shown in Fig. 6b, I_p is indeed proportional to $v^{1/2}$, confirming a diffusion-controlled behavior. From the slope of the lines and based on Eq. (1), the diffusion coefficients D_a (a peak) and $D_{a'}$ (a' peak) can be calculated to be 2.80×10^{-11} $cm^2\ s^{-1}$ and 2.42×10^{-11} $cm^2\ s^{-1}$, respectively. Such high Li-ion diffusion coefficients are related to the thin carbon-shell coated on the $LiFePO_4$ particles.

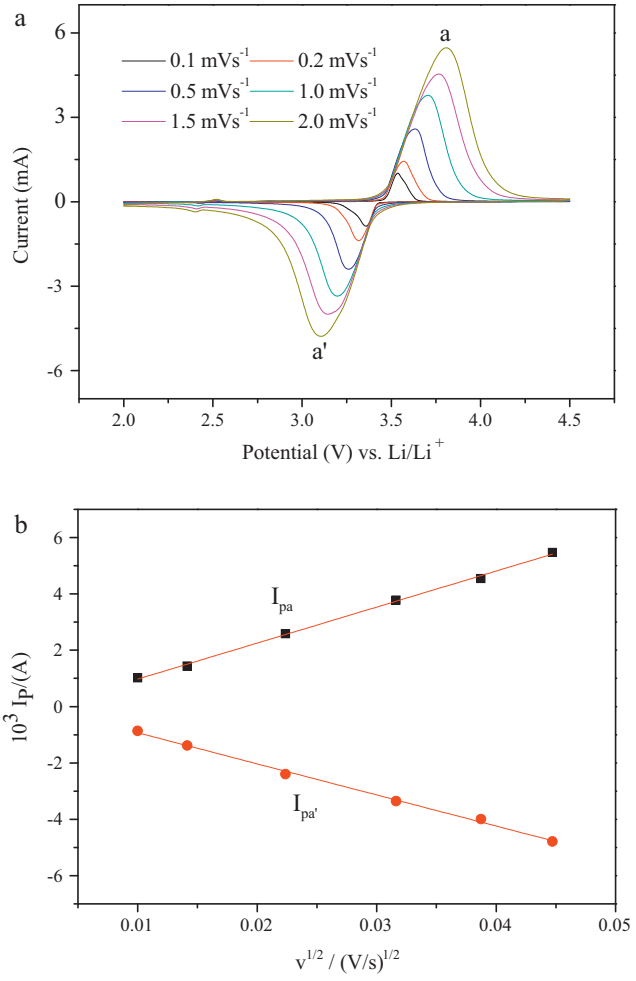

Fig. 6. (a) CV curves of $LiFePO_4$/C synthesized at 600 °C at various scanning rates between 2.0 and 4.5 V, (b) peak current I_p as a function of square root of scan rate $v^{1/2}$.

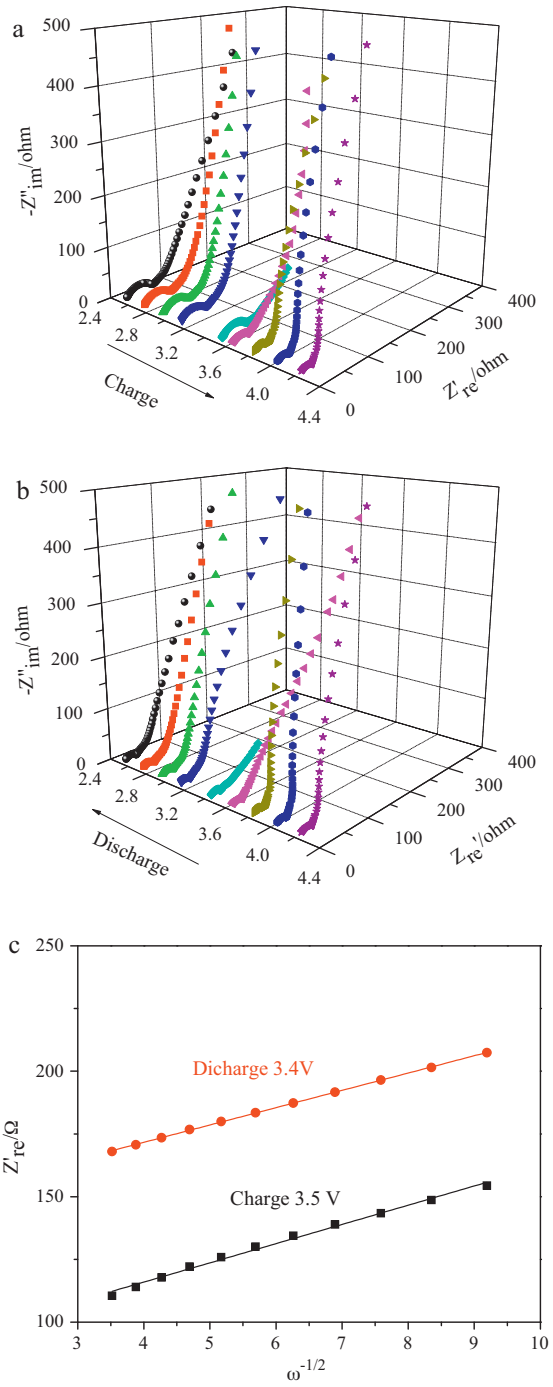

Fig. 7. Nyquist plots of the $LiFePO_4$/C synthesized at 600 °C measured under various open-circuit potentials: (a) in the state of charge, (b) in the state of discharge; (c) relationship plot between Z'_{re} and $\omega^{-1/2}$ of the material at 3.5 V (charge), 3.4 V (discharge).

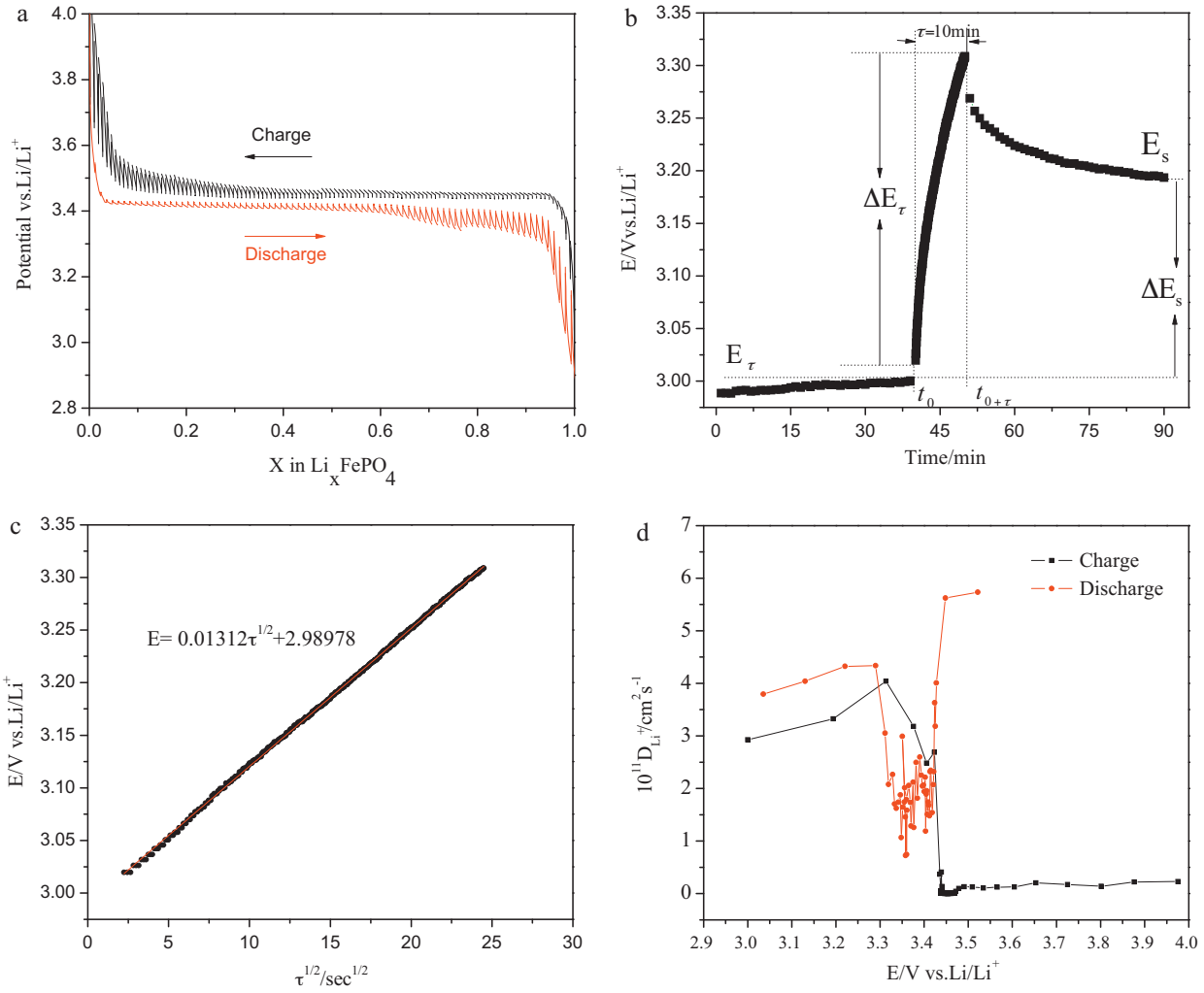

Fig. 8. (a) Charge/discharge GITT curves for $LiFePO_4$/C synthesized at 600 °C. (b) t vs. E profile of $LiFePO_4$/C for a single GITT titration. (c) Linear behavior of the E vs. $\tau^{1/2}$ relationship. (d) The plot of the lithium chemical diffusion coefficients obtained by GITT as a function of potential.

The Nyquist plots of the $LiFePO_4$/C electrode at different charge and discharge states in the first cycle are shown in Fig. 7a and b. The shape of Nyquist plots is quite different along the charge and discharge depth. At the charge states ranging from 2.5 to 3.5 V, the semicircles at high-to-middle frequency range almost overlap each other but the slopes of the low-frequency line are different. Above 3.5 V, the intercepts of the semicircles decrease with the charge states increasing from 3.6 to 4.2 V, and they become much smaller than the ones between 2.5 and 3.5 V. When discharging, all the semicircles at high-to-middle frequency range have no change, only the low-frequency lines have some differences. The characteristics of Nyquist plots at different states can reflect the changes of kinetics during the discharge–charge process.

EIS is also an important method to evaluate the diffusion coefficient of lithium ions in electrode material since the Warburg impedance in the low frequency is directly related to the lithium-ion diffusion process. The diffusion coefficient of lithium ions can be calculated from the plots in the low frequency region using the following equation [45–47]:

$$D_{Li^+} = \frac{R^2T^2}{2A^2n^4F^4C^2\sigma^2} \quad (2)$$

where R is the gas constant, T is the absolute temperature, A is the interface between the electrolyte and the active material, n is the number of electrons per molecule during oxidization, F is the Faraday constant, C is the concentration of lithium-ion, and σ is the Warburg factor which has relationship with Z'_{re}:

$$Z'_{re} = R_e + R_{ct} + \sigma\omega^{-1/2} \quad (3)$$

where R_e is the resistance of the electrolyte, and R_{ct} is the charge transfer resistance and ω is the angular frequency in the low frequency region. Here we only investigate the Li^+ diffusion behavior at the charge plateaus (3.5 V vs. Li/Li^+) and discharge plateaus (3.4 V vs. Li/Li^+). Fig. 7c shows the relationship between Z'_{re} and square root of frequency ($\omega^{-1/2}$) in the low frequency region. Thus, based on Eq. (2), the apparent diffusion coefficients of Li ions in the $LiFePO_4$/C electrode at the charge and discharge state are 1.97×10^{-13} and 2.43×10^{-13} $cm^2\ s^{-1}$, respectively, which are lower than those by CV.

Meanwhile, GITT is also used to evaluate the lithium interclation–deinterclation process in the $LiFePO_4$/C electrode. Fig. 8a shows the GITT curves of $LiFePO_4$/C in the first charge and discharge state. The chemical diffusion coefficient of Li ions (D_{Li^+}) is calculated according to Eq. (4) derived by Weppner and Huggins [48]:

$$D_{Li^+} = \frac{4}{\pi}\left(\frac{mV_M}{MA}\right)^2\left(\frac{\Delta E_s}{\tau(dE_\tau/d\sqrt{\tau})}\right)^2\left(\tau \ll \frac{L^2}{D_{Li^+}}\right) \quad (4)$$

where V_M is the molar volume of the compound, M and m are the molecular weight and mass of the $LiFePO_4$/C, respectively, A is the

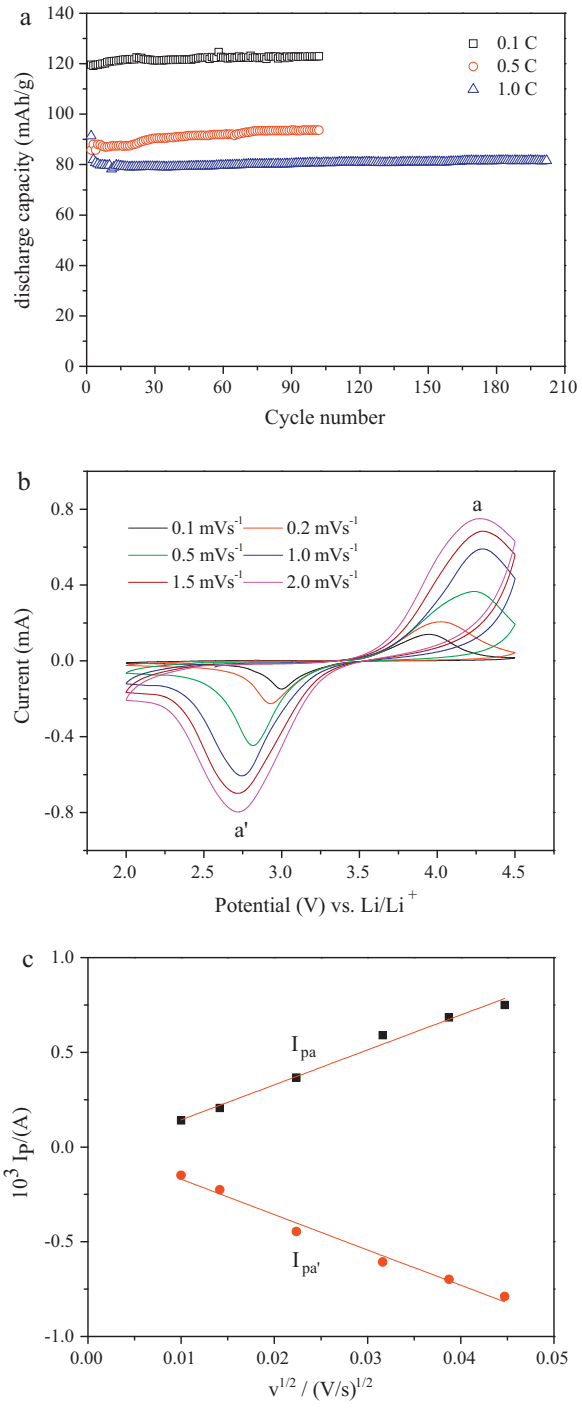

Fig. 9. (a) Cycling performance of $LiFePO_4$/C synthesized at 600 °C tested at −20 °C at different rates. (b) CV curves of $LiFePO_4$/C synthesized at 600 °C tested at −20 °C at various scanning rates between 2.0 and 4.5 V. (c) Peak current I_p as a function of square root of scan rate $v^{1/2}$ tested at −20 °C.

interface between the electrolyte and the active material, and L is the radius of the active material particle. If E versus $\tau^{1/2}$ shows a straight line behavior over the entire time period of current flux (as shown in Fig. 8c), Eq. (4) can be further simplified as [48]:

$$D_{Li^+} = \frac{4}{\pi\tau}\left(\frac{mV_M}{MA}\right)^2\left(\frac{\Delta E_s}{\Delta E_\tau}\right)^2 \quad (5)$$

Fig. 8b shows a typical t versus E profile for a single titration. Based on Eq. (5) and GITT measurement, we can obtain the diffusion coefficients of Li ions at varying voltages, as seen from Fig. 8d. The diffusion coefficients calculated from GITT at different voltages are in the range of 10^{-11}–10^{-14} $cm^2\ s^{-1}$. In the range of 3.40–3.55 V, the values of diffusion coefficient during discharge process are much higher than those during charge process. This may be because that the potential dropped to 3.52 V after the first open circuit stand during discharge process for 40 min.

For EV, batteries are required to operate at low temperature. Fig. 9a shows the cycle performance of the $LiFePO_4$/C electrode synthesized at 600 °C operated at low temperature. The $LiFePO_4$/C electrode exhibits excellent cycle stability at various current rates at −20 °C. While cycling at 0.1 C, 0.5 C and 1 C rate, it delivers an initial discharge capacity of 122, 90 and 80 mAh g^{-1}, respectively. The $LiFePO_4$/C electrode has not any fading after 200 cycles at 1 C, and 100 cycles at 0.5 C and 0.1 C, respectively. Fig. 9b shows the CV curves of the $LiFePO_4$/C electrode tested at −20 °C. The redox peaks become smooth and the polarization increases compared with the CV tested at room temperature. Based on Eq. (1) and Fig. 9c, it can be obtained that the diffusion coefficients are 4.07×10^{-12} and 4.11×10^{-12} $cm^2\ s^{-1}$ at the oxidation and reduction states, respectively.

4. Conclusions

In summary, a core–shell structured $LiFePO_4$/C nanocomposite was synthesized by the solid state reaction route using PVA as carbon source. This composite has a thin carbon-shell (about 1.3 nm) which coats completely on the inner $LiFePO_4$. The $LiFePO_4$/C nanocomposite could get electrons from all directions and the Li^+ ions could penetrate through the carbon-shell without appreciable polarization. Therefore, the rate capability of the lithium insertion reaction and the electrochemical performance were improved significantly, especially at high charge–discharge rates. At a low temperature of −20 °C, the $LiFePO_4$/C nanocomposite also exhibited good cycle performance. In addition, such low carbon content can enhance energy density of the materials significantly.

References

[1] A.S. Arico, P. Bruce, B. Scrosati, J.-M. Tarascon, W. van Schalkwijk, Nat. Mater. 4 (2005) 366.
[2] S. Bashash, S.J. Moura, J.C. Forman, H.K. Fathy, J. Power Sources 196 (2011) 541.
[3] G. Armstrong, A.R. Armstrong, P.G. Bruce, P. Reale, B. Scrosati, Adv. Mater. 18 (2006) 2597.
[4] C. Wadia, P. Albertus, V. Srinivasan, J. Power Sources 196 (2011) 1593.
[5] X.H. Huang, J.P. Tu, B. Zhang, C.Q. Zhang, Y. Li, Y.F. Yuan, H.M. Wu, J. Power Sources 161 (2006) 541.
[6] X.H. Huang, J.P. Tu, X.H. Xia, J.Y. Xiang, X.L. Wang, J. Power Sources 195 (2010) 1207.
[7] B. Scrosati, Nature 373 (1995) 557.
[8] A.K. Padhi, K.S. Nanjundaswamy, J.B. Goodenough, J. Electrochem. Soc. 144 (1997) 1188.
[9] X.H. Rui, C. Li, C.H. Chen, Electrochim. Acta 54 (2009) 3374.
[10] D.Y. Wang, H. Li, S.Q. Shi, X.J. Huang, L.Q. Chen, Electrochim. Acta 50 (2005) 2955.
[11] C. Delacourt, P. Poizot, J.M. Tarascon, C. Masquelier, Nat. Mater. 4 (2005) 254.
[12] C. Delacourt, P. Poizot, S. Levasseur, C. Masquelier, Electrochem. Solid-State Lett. 9 (2006) A352.
[13] M.M. Doeff, Y.Q. Hu, F. McLarnon, R. Kostecki, Electrochem. Solid-State Lett. 6 (2003) A207.
[14] K. Zaghib, J. Shim, A. Guerfi, P. Charest, K.A. Striebel, Electrochem. Solid-State Lett. 8 (2005) A207.
[15] G.Y. Chen, X.Y. Song, T.J. Richardson, Electrochem. Solid-State Lett. 9 (2006) A295.
[16] J.Y. Xiang, J.P. Tu, L. Zhang, X.L. Wang, Y. Zhou, Y.Q. Qiao, Y. Lu, J. Power Sources 195 (2010) 8331.
[17] V. Srinivasan, J. Newman, Electrochem. Solid-State Lett. 9 (2006) A110.
[18] P.S. Herle, B. Ellis, N. Coombs, L.F. Nazar, Nat. Mater. 3 (2004) 147.
[19] M.M. Thackeray, J. Power Sources 7 (2001) 97.
[20] H. Huang, S.C. Yin, L.F. Nazar, Electrochem. Solid-State Lett. 4 (2001) A170.
[21] F. Croce, A.D. Epifanio, J. Hassoun, A. Deptula, T. Olczac, B. Scrosati, Electrochem. Solid-State Lett. 5 (2002) A47.

[22] Q. Wang, S.M. Zakeeruddin, D. Wang, I. Exnar, M. Grätzel, Angew. Chem. Int. Ed. 45 (2006) 8197.
[23] L.X. Yuan, Z.H. Wang, W.X. Zhang, X.L. Hu, J.T. Chen, Y.H. Huang, J.B. Goodenough, Energy Environ. Sci. 4 (2011) 269.
[24] Y.K. Zhou, J. Wang, Y.Y. Hu, R. O'Hayre, Z.P. Shao, Chem. Commun. 46 (2010) 7151.
[25] F. Yu, J.J. Zhang, Y.F. Yang, G.Z. Song, J. Power Sources 195 (2010) 6873.
[26] X.L. Wu, L.Y. Jiang, F.F. Cao, Y.G. Guo, L.J. Wan, Adv. Mater. 21 (2009) 2710.
[27] G.X. Wang, H. Liu, J. Liu, S.Z. Qiao, G.M. Lu, P. Munro, H.J. Ahn, Adv. Mater. 22 (2010) 4944.
[28] J.F. Qian, M. Zhou, Y.L. Cao, X.P. Ai, H.X. Yang, J. Phys. Chem. C 114 (2010) 3477.
[29] J. Liu, T.E. Conry, X.Y. Song, M.M. Doeff, T.J. Richardson, Energy Environ. Sci. 4 (2011) 885.
[30] M.H. Lee, J.Y. Kim, H.K. Song, Chem. Commun. 46 (2010) 6795.
[31] B.L. Ellis, M. Wagemaker, F.M. Mulder, L.F. Nazar, Adv. Funct. Mater. 20 (2010) 186.
[32] W.J. Zhang, J. Electrochem. Soc. 157 (2010) A1040.
[33] Y.G. Wang, Y.R. Wang, E.J. Hosono, K.X. Wang, H.S. Zhou, Angew. Chem. Int. Ed. 47 (2008) 7461.
[34] R. Dominko, M. Bele, M. Gaberscek, M. Remskar, D. Hanzel, S. Pejovnik, J. Jamnik, J. Electrochem. Soc. 152 (2005) A607.
[35] R. Dominko, M. Bele, J.-M. Goupil, M. Gaberscek, D. Hanzel, I. Arcon, J. Jamnik, Chem. Mater. 19 (2007) 2960.
[36] C.M. Doherty, R.A. Caruso, B.M. Smarsly, C.J. Drummond, Chem. Mater. 21 (2009) 2895.
[37] Z.H. Chen, J.R. Dahn, J. Electrochem. Soc. 149 (2002) A1184.
[38] N.J. Yun, H.-W. Ha, K.H. Jeong, H.-Y. Park, K. Kim, J. Power Sources 160 (2006) 1361.
[39] F. Gao, Z.Y. Tang, H.J. Xue, Electrochim. Acta 53 (2007) 1939.
[40] B. Zhao, Y. Jiang, H.J. Zhang, H.H. Tao, M.Y. Zhong, Z. Jiao, J. Power Sources 189 (2009) 462.
[41] S.H. Luo, Z. Tang, J.B. Lu, Z.T. Zhang, Ceram. Int. 34 (2008) 1349.
[42] D. Jugovic, M. Mitric, N. Cvjeticanin, B. Jancar, S. Mentus, D. Uskokovic, Solid-State Ionics 179 (2008) 415.
[43] W. Gilman Jeffrey, L. VanderHart David, T. Kashiwagi, Fire and Polymers II, American Chemical Society, 1995, p. 161.
[44] A.J. Bard, L.R. Faulkner, Electrochemical Methods, 2nd ed., Wiley, New York, 2001, p. 226.
[45] R.H. Zeng, W.S. Li, D.S. Lu, Q.M. Huang, J. Power Sources 174 (2007) 592.
[46] Y. Cui, X.L. Zhao, R.S. Guo, Electrochim. Acta 55 (2010) 922.
[47] J.Y. Xiang, J.P. Tu, Y.Q. Qiao, X.L. Wang, J. Zhong, D. Zhang, C.D. Gu, J. Phys. Chem. C 115 (2011) 2505.
[48] W. Weppner, R.A. Huggins, J. Electrochem. Soc. 124 (1977) 1569.